



Insights on aggregation induced room temperature phosphorescence properties: A QM/MM study

Yuchen Zhang, Yuying Ma, Kai Zhang, Chuan-Kui Wang^{**}, Lili Lin^{***}, Jianzhong Fan^{*}

Shandong Province Key Laboratory of Medical Physics and Image Processing Technology, School of Physics and Electronics, Shandong Normal University, 250014, Jinan, China

ARTICLE INFO

Keywords:

Room temperature phosphorescence
Aggregation induced emission
Dimer emission
QM/MM method

ABSTRACT

Organic room temperature phosphorescence (RTP) molecules have attracted significant attention recently due to their promising application in security, bioimaging, sensing and organic light emitting diodes (OLEDs). Nevertheless, limited RTP molecules were reported until now and most of RTP phenomena were observed in crystal. Moreover, the underlying mechanisms of RTP still remain ambiguous. In this paper, excited-state properties of CZs-CN with RTP features in three crystals are theoretically studied using the combined quantum mechanics and molecular mechanics (QM/MM) method. Moreover, the photophysical properties of CZs-CN in solvent are also investigated by polarizable continuum model (PCM). The mechanism of aggregation induced RTP is revealed which is mainly contributed by the enhanced phosphorescence rates in aggregation, rather than the traditional restricted intramolecular motion mechanisms which usually bring decreased non-radiative decay rates. In addition, different crystal structures could induce different phosphorescence properties, and the emission spectra of the molecule in three crystals and THF are explained reasonable. Furthermore, dimers are confirmed to be involved in the emission when the intermolecular interaction is strong enough in aggregation. Our theoretical results provide inner perspective for aggregation induced RTP mechanism and could help one to better understand the different light-emitting properties in aggregation and solvent.

1. Introduction

Organic light-emitting diodes (OLEDs) possess many attractive features for lighting and display. They emit spontaneous light and can be light weight, ultra-thin, and flexible. In OLEDs, 75% of excitons generated are triplets and the singlet excitons only account for 25% in electroluminescence. This means that the process of highest internal quantum efficiency by traditional fluorescence emission is limited to 25% in OLEDs [1–6]. In order to take advantage of all excitons, phosphorescence materials are developed. In the conventional view, a phosphorescent emitter possesses large spin-orbit coupling (SOC) when heavy metals are added. However, the addition of heavy metals in the organic matrix increases the costs and causes severe environmental pollution. In addition, phosphorescence often needs to be observed at low temperature (77 K), because non-radiative process can be suppressed at low temperature. That way, triplet excitons return to the ground state (S_0) through the radiative channel. Furthermore, organic

room temperature phosphorescence (RTP) materials broke the requirement of a cold environment for traditional phosphorescence and the need for heavy metals, so that 100% excitons can be used [7–12]. RTP materials show promising applications for the next-generation OLEDs and many efforts have been devoted to this area. Tang et al. realized 3D printing with a single RTP molecule producing white emission [13]. Tian et al. developed a pure organic polymer for an efficient heavy-atom-free RTP emission with a lifetime of 537 ms and a quantum yield of 15.39% [14]. Huang et al. achieved ultra-long organic phosphorescence (UOP) by manipulating intermolecular interactions caused by H-aggregation that stabilize the excited triplet state with a high phosphorescence efficiency of 8.3% and a considerably long lifetime of 0.84 s [15]. Ma, Peng and Shuai proposed theoretical descriptors of γ and β for designing high efficiency and long-lived RTP molecules, the concomitant relationships between the descriptors and phosphorescence efficiency and lifetime are illustrated [16–18].

Despite the explosive growth in this research field, a crucial reason

* Corresponding author.

** Corresponding author.

*** Corresponding author.

E-mail addresses: ckwang@sdnu.edu.cn (C.-K. Wang), linli@sdnu.edu.cn (L. Lin), fanjianzhongvip@163.com (J. Fan).

for inefficient RTP is the deactivation of triplet states caused by molecular vibration and rotation relaxation. Thus, many methods have been applied to boost the efficiency and lifetime, such as the host-guest doping, crystallization, molecular self-assembly, metal-organic frameworks (MOF) and so on [19–24]. Furthermore, in 2001, Tang et al. discovered the phenomenon of aggregation induced emission (AIE), which not only enables the luminous molecules to glow in the aggregation state but also greatly enhances the luminous efficiency [25,26]. Thus, the AIE material becomes an ideal candidate for the preparation of non-doped OLEDs and the first RTP materials derived from the exact AIE was reported by Tang and coworkers [27]. The use of AIE materials improves the device efficiency and stability, and shows different luminescence characteristics from different stacking modes, virtually making a shining bridge between the macro and the micro world. Moreover, the combination with the high exciton utilization of RTP will definitely lead to a new peak of luminescent materials in the future [28–31]. However, the mechanism of AIE in RTP emitter is still unclear. One particular ongoing interest is the enhanced emission of dyes in viscous and solid-state environments.

Recently, Li et al. synthesized a new RTP molecule named CzS-CN (Fig. 1) with AIE properties [32]. They integrated a phenothiazine and benzo nitrile moiety to yield a new RTP luminogen. Three crystalline polymorphs were cultured through simple slow solvent evaporation from different initial solutions. The Crystal A, Crystal B and Crystal C show different RTP lifetimes of 266 ms, 41 ms, and 32 ms, accompanied by different photoluminescence (PL) quantum yields of 22.6%, 17.8% and 6.9%, respectively. All these properties are related to molecular packing effect. Therefore, a theoretical investigation to reveal the influence of intermolecular packing on the properties of RTP and AIE is desired.

In this work, we perform detailed studies on the latest reported RTP molecule CzS-CN, based on first-principles calculations. Photophysical properties of CzS-CN in tetrahydrofuran (THF) are theoretically investigated by using the polarizable continuum model (PCM) [33]. In order to take the environment of the molecule in the solid phase into consideration, the combined quantum mechanics and molecular

mechanics (QM/MM) method is adopted [34–38]. Moreover, the independent gradient model (IGM) method is used to visualize the intermolecular interactions and the intensity of interaction is compared by energy decomposition analysis. Furthermore, the non-radiative rate as well as the intersystem crossing (ISC) and reverse intersystem crossing (RISC) rates are calculated by the thermal vibration correlation function (TVCF) and the Marcus equation, respectively. Finally, the dynamics of the excited state are investigated and the RTP as well as AIE mechanisms are illustrated, experimental measurements are reasonably explained.

2. Methodology

Geometric structures of CzS-CN (Fig. 1(a)) in ground state (S_0) and excited states are optimized using the density functional theory (DFT) method and the time-dependent density functional theory (TD-DFT) respectively. Since the CzS-CN molecule is composed of donor and acceptor groups, its excited-state properties are dependent on the functionals adopted. Here, functionals with different Hartree-Fock components are tested. The fluorescent emission wavelengths of CzS-CN with different crystal structures (A, B, C) are calculated and compared with experimental values (as shown in Table 1). It can be found that the fluorescent emission wavelengths of CzS-CN calculated with B3LYP functional are 346 nm, 414 nm and 375 nm respectively for crystal A, B and C, and they are in better agreement with experimental

Table 1

Emission wavelengths calculated by adopting different functionals for studied molecule in solid phase.

	HF (%)	Crystal A(nm)	Crystal B(nm)	Crystal C(nm)
B3LYP	20	346	414	375
PBE0	25	333	380	349
BMK	42	308	300	311
WB97XD	–	296	314	296
Exp*	—	410	430	380

Exp* is experimental data.

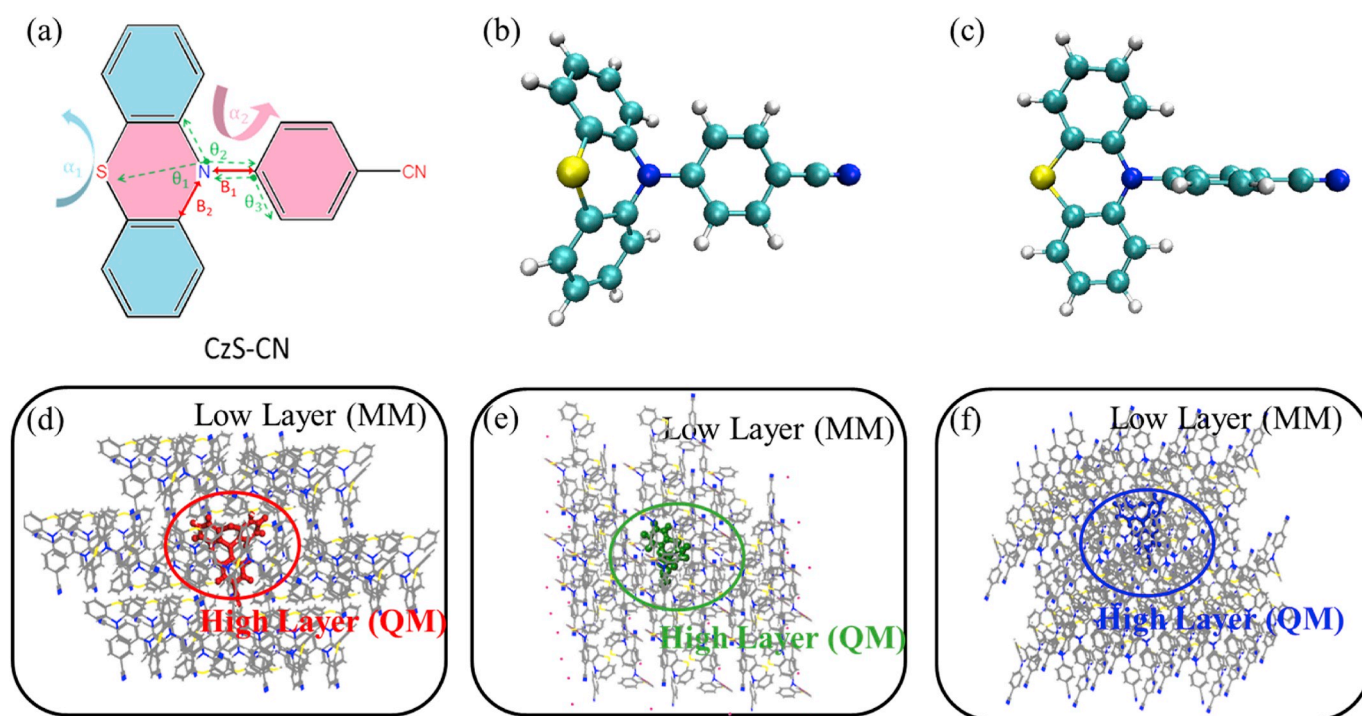


Fig. 1. (a) Chemical structure of CzS-CN. Interesting bond lengths, bond angles, and dihedral angles are marked. The stable geometries in THF of CzS-CN-ax (b) and CzS-CN-eq (c). ONIOM model for Crystal A (d), Crystal B (e) and Crystal C (f), respectively.

values (410 nm, 430 nm and 380 nm) quantitatively than with other functionals. It indicates that the B3LYP functional is suitable for the describing the excited properties of CzS-CN. As for the calculation of CzS-CN in crystal A, B and C, the combined quantum mechanics and molecular mechanics (QM/MM) method with two-layer ONIOM approach is used. The two layers ONIOM model is constructed from the crystal structure and is shown in Fig. 1(d)–(f) [39]. The initial structure is built based on the crystal structure detected experimentally [32]. The central single molecule is regarded as the high layer and calculated by the QM method. The surrounding molecules are treated as the MM part, which is defined as the low layer. The universal force field (UFF) is adopted for the MM part and the electronic embedding is selected in our QM/MM calculations. In addition, molecules of the MM part are frozen during the geometry optimizations for S_0 , the first singlet excited state (S_1) and the first triplet excited state (T_1). The B3LYP/6-31G (*) level is used in all the QM calculations. All these calculations above are performed with the Gaussian 16 package [40].

Furthermore, based on the obtained electronic structure and vibration information, the normal mode analysis is performed with the DUSHIN program [41], and the Huang-Rhys (HR) factor and the reorganization energy contributed from vibration modes are analyzed. The spin-orbit coupling (SOC) is calculated with the Dalton2013 package [42]. The fluorescent radiative rate is calculated using the Einstein spontaneous emission formula

$$k_r = \frac{f \Delta E_{ji}^2}{1.499 \text{ cm}^{-2} \text{ s}} \quad (1)$$

Where f is the oscillator strength of S_1 . ΔE_{ji} is the energy gap between S_1 and S_0 in unit of wavenumber (cm^{-1}). As for phosphorescent rate, it is calculated based on the equation

$$K_r(T_m \rightarrow S_0) \approx \frac{16\pi^3 10^6 n^3 E(T_m)^3}{3h\varepsilon_0} \left\{ \sum_n \frac{\langle T_m | H_{SOC} | S_n \rangle \langle S_n | M | S_0 \rangle}{E(S_n) - E(T_m)} \right\}^2 \quad (2)$$

Here n and ε_0 are refractive index of the medium and the permittivity in vacuum, respectively. $E(S_n)$ and $E(T_m)$ denote the excitation energy from the n th singlet state (S_n) and m th triplet state (T_m) to S_0 . $\langle S_n | M | S_0 \rangle$ is the transition dipole moment from S_n to S_0 .

Finally, the radiative and non-radiative decay rates of studied molecules from T_1 to S_0 are calculated by TVCF method applied in MOMAP package, due to their RTP properties. Detail calculation information can refer to Ref. [43–45]. The intersystem crossing rates are calculated with the Marcus equation [46–48].

3. Results and discussions

For the CzS-CN molecule, three different crystal structures are obtained and different emission properties were found. Both the stacking structures and molecular geometry may influence the emission properties. The geometry parameters of the molecule in Crystal A, B and C are listed in Table 2. All the parameters' definition is shown in Fig. 1 (a). We

can find that the geometry of the molecule in Crystal A is close to that in Crystal B. However, the geometry of the molecule in Crystal C has relative larger discrepancy compared with that in Crystal A and B. The main differences come from the angles: α_1 is larger and α_2 is smaller. The angles θ_1 also has significant difference. Although there are some changes for the molecular geometry after optimization, they are still quite close to the geometry of the crystals respectively. Nevertheless, the molecular geometry in solvent after optimization is quite different from that in Crystals. Actually, two stable geometries are found for the molecule in solvent. We found that configuration CzS-CN-ax (quasi-axial) is close to the geometry in crystals (as shown in Fig. 1(e)), while configuration CzS-CN-eq (quasi-equatorial) is quite different from them. The angle of α_2 becomes 82° , which means that the donor (D) group and the acceptor (A) group close to perpendicular to each other. Large angle between D and A will induce significant charge transfer (CT) state and small energy gap between the first excited singlet state (S_1) and the first excited triplet state (T_1). Since emissions of molecules are usually dependent on S_1 and T_1 , the geometry of both S_1 and T_1 are also optimized. The geometric parameters are also listed in Table 2. It is found that the geometry of both S_1 and T_1 have some differences with that in ground state (S_0). The changes of the molecule during excitation in THF solvent are more obvious than that in crystals. These changes are measured by root of the mean of squared displacement (RMSD) with the

expression of $\text{RMSD} = \sqrt{\frac{1}{N} \sum_i^{\text{natom}} [(x_i - x'_i)^2 + (y_i - y'_i)^2 + (z_i - z'_i)^2]}$, corresponding results between S_0 , S_1 and T_1 are shown in Fig. 2. The RMSD values for S_0 vs. S_1 , S_1 vs. T_1 and S_0 vs. T_1 are 1.631 Å, 1.527 Å and 0.271 Å in THF respectively, and they decrease to 0.103 Å, 0.077 Å and 0.087 Å. Thus, geometry changes in THF are more obvious.

In addition, since two configurations were found for the molecule in THF, we began to wonder whether two configurations can change conformers easily. The scanned potential energy curve with different angles (α_2) are shown in Fig. 3. It can be found that both configurations are local minimum in the potential energy curve with CzS-CN-ax lower in energy. The energy barrier from CzS-CN-ax to CzS-CN-eq is about 3.77 kcal/mol, while the reverse energy barrier from CzS-CN-eq to CzS-CN-ax is only 1.81 kcal/mol. So the molecule tends to exist in the form of CzS-CN-ax in THF solution. Furthermore, the emission wavelengths of both S_1 and T_1 are calculated for the molecule in crystals and solvent respectively. The calculated fluorescent and phosphorescent wavelengths for the molecule in crystal A, B and C are all in good agreement with experimental values except for the fluorescent wavelength of the molecule in crystal A. For the emissions in THF, the calculated fluorescent wavelength and phosphorescent wavelength of CzS-CN-ax are in good agreement with experimental values, which indicates that the emission of the molecule in THF should come from CzS-CN-ax. The calculated fluorescent wavelength and phosphorescent wavelength of CzS-CN-eq has a large discrepancy with experimental values, thus the emission detected experimentally should not come from CzS-CN-eq. Then two questions show up: one is that why CzS-CN-eq does not

Table 2

Geometrical parameters of A, S_0 , S_1 , and T_1 states in solid phase and THF. α , θ and B (marked in Fig. 1 (a)) represent the dihedral angle, bond angle and bond length, respectively (A is the initial value).

	Crystal A				Crystal B				Crystal C				THF (CzS-CN-ax)			THF (CzS-CN-eq)		
	A	S_0	S_1	T_1	A	S_0	S_1	T_1	A	S_0	S_1	T_1	S_0	S_1	T_1	S_0	S_1	T_1
$\alpha_1(^{\circ})$	44	46	44	46	49	43	37	44	57	59	55	59	49	41	50	32	0	0
$\alpha_2(^{\circ})$	62	67	60	65	64	61	62.8	55.4	55	51	50	50	57	40.5	44	82	90	90
$\theta_1(^{\circ})$	117	121	118	118	116	115	119	115	127	121	117	119	122	143	138	161	180	180
$\theta_2(^{\circ})$	119	120	121	122	119	121	116	121	123	123	121	122	122	122	123	118	118	118
$\theta_3(^{\circ})$	121	116	129	131	121	119	133	132	122	130	142	137	121	121	121	121	120	120
$B_1(\text{\AA})$	1.39	1.41	1.38	1.41	1.43	1.41	1.51	1.41	1.40	1.40	1.49	1.40	1.40	1.46	1.41	1.44	1.45	1.45
$B_2(\text{\AA})$	1.44	1.43	1.44	1.42	1.41	1.43	1.39	1.42	1.43	1.43	1.39	1.42	1.43	1.40	1.43	1.42	1.39	1.40

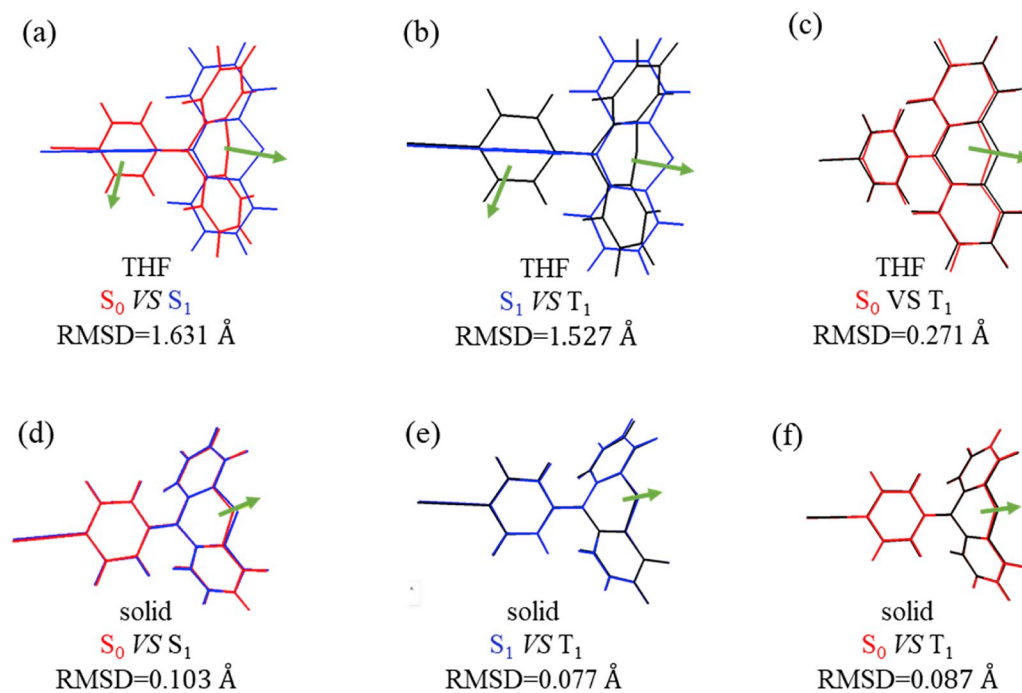


Fig. 2. Geometry comparisons between S_0 (red), S_1 (blue) and T_1 (black) in THF (a, b, c) and solid phase (d, e, f). (For interpretation of the references to colour in this figure legend, the reader is referred to the Web version of this article.)

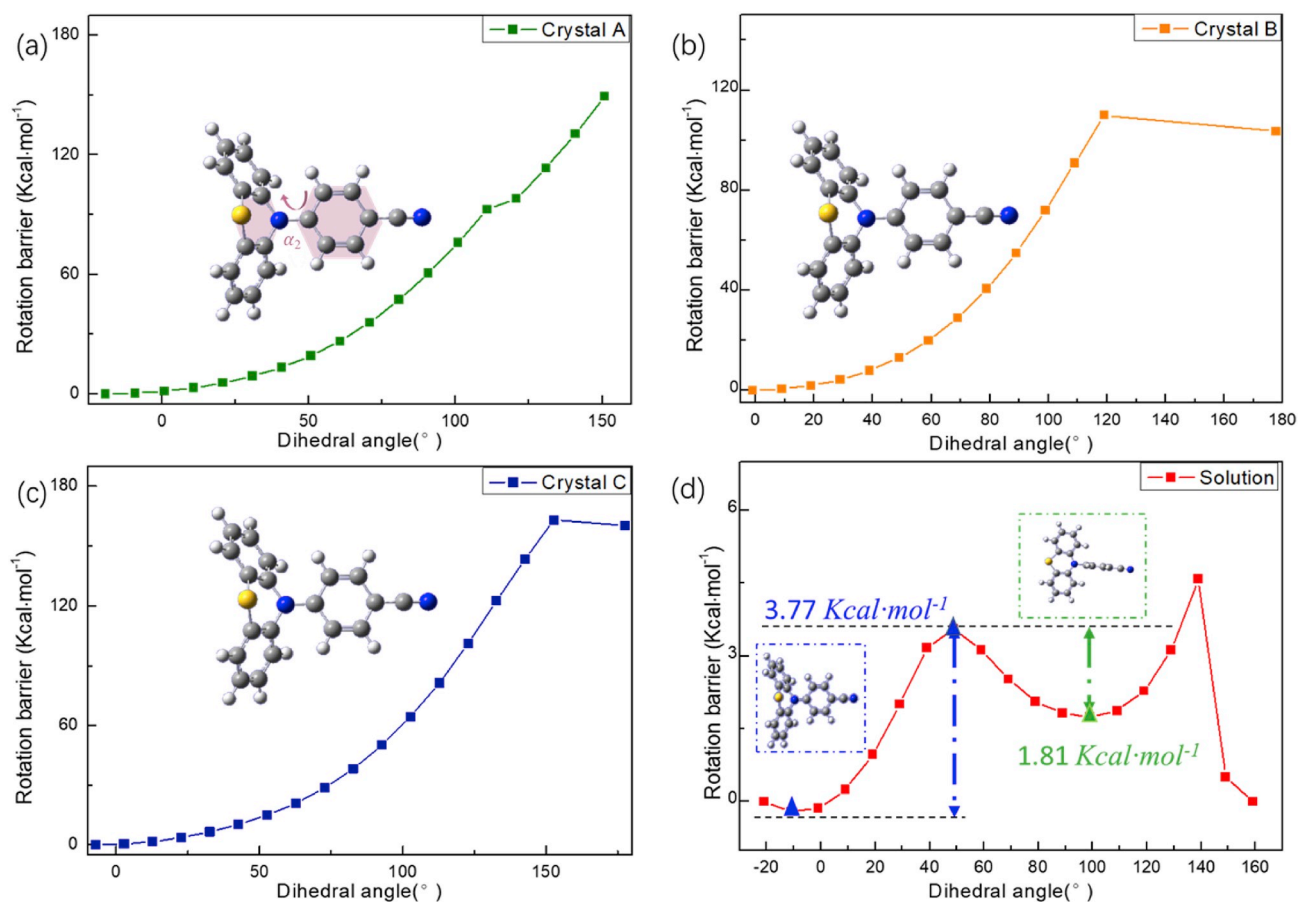


Fig. 3. The potential energy surface scan varies with the dihedral angle (α_2) for the molecule in Crystal A (a), Crystal B (b), Crystal C (c) and THF (d), respectively.

contribute to fluorescence and phosphorescence; the other is why the calculated emission wavelength of the molecule in crystal A does not agree with experimental values.

In order to explore the abovementioned two issues, the scanned potential energy curves of the molecule in S_1 and T_1 in THF solvent are calculated and plotted in Fig. 4 (a), where the angle α_2 is changed. It can be found that both S_1 and T_1 for CzS-CN-eq are more stable than CzS-CN-ax. The energy barrier from CzS-CN-ax to CzS-CN-eq is 1.09 kcal/mol for T_1 and no barrier is found for S_1 . Thus, it is easy for CzS-CN-ax transformed to CzS-CN-eq in excited states. In order to explain the emission from CzS-CN-eq cannot be detected. The calculated oscillator strength for CzS-CN-eq is zero, which means that CzS-CN-eq should not decay by emission. Considering close energy levels between S_1 and T_1 , it is quite possible that the molecule converted to T_1 by RISC process. Since the phosphorescence emission from CzS-CN-eq cannot be detected due to the vanished SOC effect with the calculated SOC value is zero and the corresponding value is 0.78 cm^{-1} for CzS-CN-ax. Moreover, the energy barrier in T_1 is about 4.36 kcal/mol , the back-conversion from CzS-CN-eq to CzS-CN-ax is also not too difficult. Thus, we predict that the emission may come from CzS-CN-ax. In addition, the participation of high excited triplet states may help the back-conversion to T_1 in CzS-CN-ax due to their small energy gaps, which further facilitate the phosphorescence emission, corresponding data are shown in Fig. 4(b). The participation of excited triplet states may help the back-conversion to T_1 in CzS-CN-ax, which will help the phosphorescence emission. Based on the analysis above, we conclude that CzS-CN-ax is responsible for the fluorescence emission, however the emission is quite weak due to the decay of S_1 to CzS-CN-eq that has no emission. The phosphorescence emission should also mainly come from CzS-CN-ax due to the interconversion between S_1 and higher excited triplet states.

To figure out the difference between the calculated fluorescence wavelength of the molecule in Crystal A and that detected experimentally, we performed potential energy curve scanned when the angle α_2 is rotated. It is found that the energy becomes higher when the angle changed, which means that it is difficult for the molecule to exist with another configuration in crystals. We checked three crystal structures of the molecule and detailed analyses for dimers are performed based on IGM method by Multiwfn [49,50], results are shown in Fig. 5 and crowded stacking pattern in Crystal A can be found. Moreover, the closest dimers taken from each crystal are studied in detail. There are significant CH- π interaction in dimers of Crystal A and B, while significant π - π interaction is found in dimers of Crystal C. The interaction energy between two molecules is calculated based on force field method. The interaction energy for dimers in Crystal A is as high as -59.7 kJ/mol , which is much larger than the interaction energy for dimers in Crystal B and C (-30.21 kJ/mol and -24.85 kJ/mol). Consequently, we guess that

excimer may contribute to emission in Crystal A. We performed calculation of dimers and found that the emission wavelength from dimers in Crystal A is 384 nm , which is in better agreement with experimental values. We conclude that dimers in Crystal A may also contribute to emission. Thus, abovementioned two questions are reasonably explained.

Moreover, the low-lying excited states have close relationship with emission properties of molecules, thus several adiabatic excitation levels of the molecule in three crystals are shown in Fig. 6. It is found that the energy gap values between S_1 and T_1 for the molecule in three crystals are 1.06 eV , 0.79 eV and 0.97 eV respectively. In addition, there are several triplet states are lower than S_1 in energy, and T_4 is close in energy to S_1 . The structure of excited states may favor the intersystem crossing (ISC) process. The energy levels for the CzS-CN-ax in THF solvent are similar to that in crystal, and with T_4 and T_5 both close to S_1 in energy. However, the S_1 - T_1 energy gap for CzS-CN-eq is 0.04 eV , which may favor both the ISC and reverse ISC process. In addition, the transition properties of all excited states involved are illustrated in Fig. 7. Since the highest occupied natural transition orbital (HONTO) and the lowest unoccupied natural transition orbital (LUNTO) mainly contribute to the transition, the electron distribution of the two orbitals are shown here. It is found that both local-excited (LE) and charge transfer (CT) properties are involved in S_1 (with LE contribution from 50% to 65%). For all the triplet states, typical LE nature is found (with LE contribution from 79% to 85%). It can also be found that the transition for triplet states mainly happens at the benzene ring and the CN unit, while both the CzS group and the CN unit are involved in the excitation of S_1 . The spin-orbit coupling (SOC) constants between S_1 and the triplet states (T_N) are calculated using the quadratic response function methods with the Dalton program (as shown in Table 3) [51]. It is found that the SOC values between S_1 and T_N for the molecule in Crystal A are a little larger than that in Crystal B and C. In addition, the SOC values between S_1 and T_1 are the smallest for the molecule in each crystal, while the values between S_1 and T_3 are the largest. Due to the smaller energy gap between S_1 and T_3 than that between S_1 and T_1 , the ISC rates between S_1 and T_3 should be larger than S_1 - T_1 ISC rate. For the SOC values in THF, the SOC between S_1 and T_1 is much smaller than that calculated in crystals. The SOC values between T_1 and S_0 are also calculated. It is found that the SOC value between T_1 and S_0 in Crystal A is also much larger than that obtained in other crystals. The T_1 - S_0 SOC value in THF solution is also much smaller than that in crystals, which predict weak phosphorescence in THF than in crystals.

Furthermore, the decay rates of the molecule in excited states are calculated (as shown in Table 4). It is found that the fluorescent rates for the molecule in crystals are smaller than that in THF solution, while the non-radiative rate for S_1 in crystals are larger than that in THF. Based on

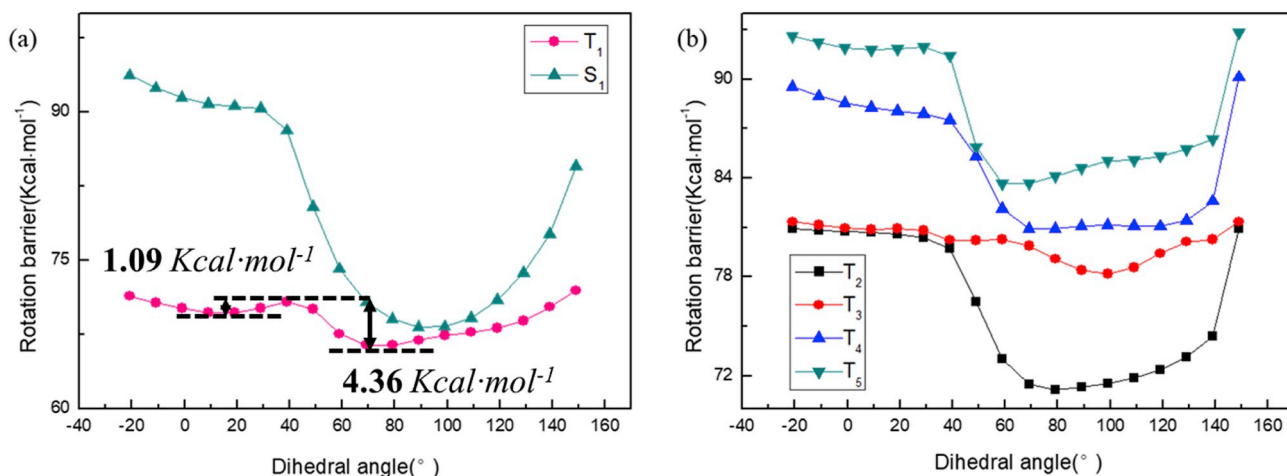


Fig. 4. The scanned potential energy curves of the molecule in S_1 , T_1 (a) and other triplet excited states (b) in THF, respectively.

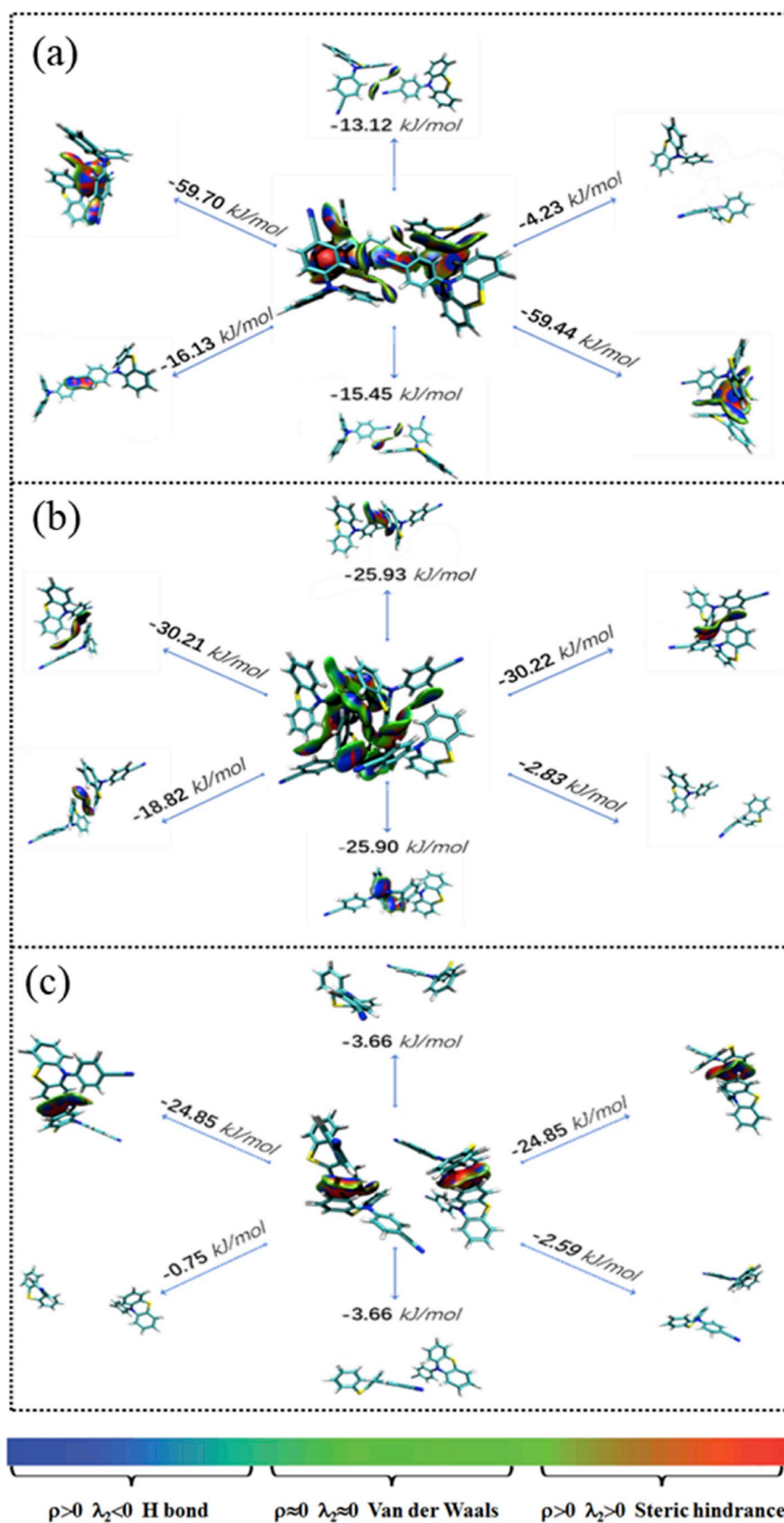


Fig. 5. Intermolecular interactions of the CzS-CN in Crystal A (a), Crystal B (b) and Crystal C (c), respectively.

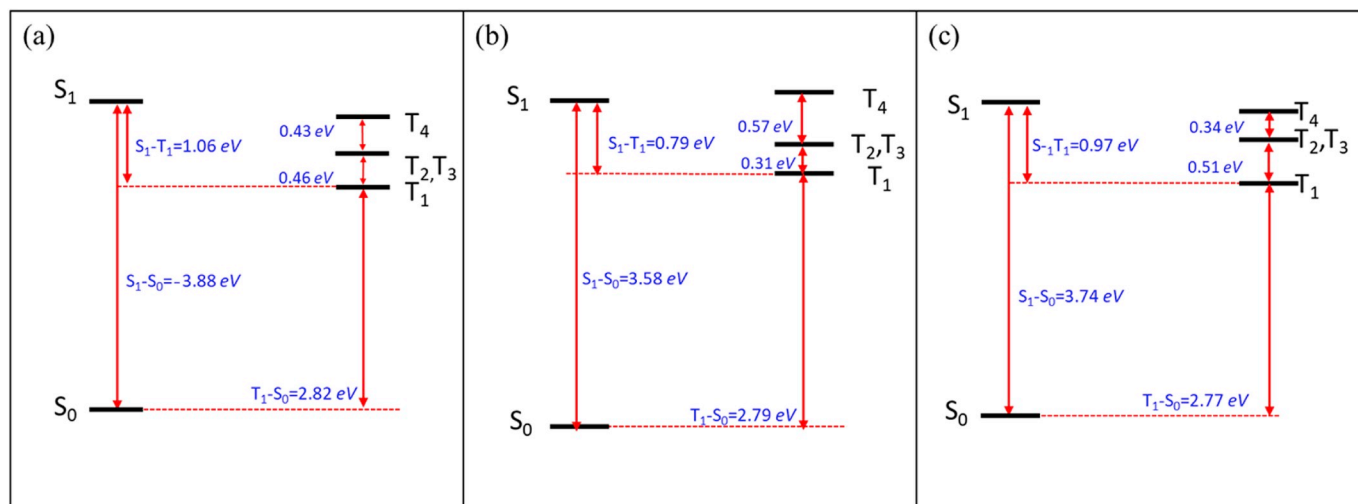


Fig. 6. Adiabatic excitation energies for CzS-CN in the Crystal A (a), Crystal B (b) and Crystal C (c), respectively.

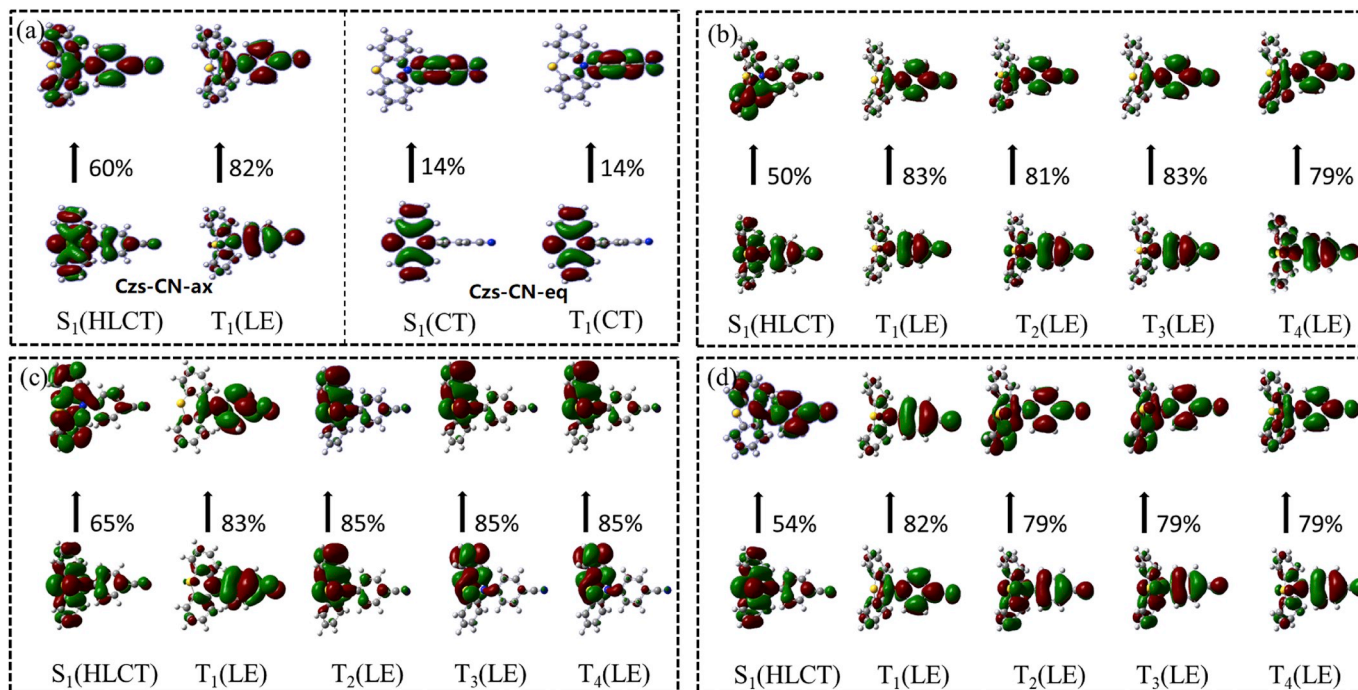


Fig. 7. Transition characteristics for S_1 and T_N states of CzS-CN in the THF (a), Crystal A (b), Crystal B (c) and Crystal C (d). The value below every arrow represents the component of localized excitation in the corresponding transition.

Table 3

Calculated spin orbit coupling constants (cm^{-1}) between selected states for molecule in Crystal A, Crystal B, Crystal C and the THF.

	Crystal A	Crystal B	Crystal C	THF
$S_1 H_{SOC} T_1$	0.47	0.36	0.36	0.02
$S_1 H_{SOC} T_2$	0.83	0.66	0.66	1.16
$S_1 H_{SOC} T_3$	1.88	1.08	1.08	1.09
$S_1 H_{SOC} T_4$	1.00	0.86	0.86	1.09
$T_1 H_{SOC} S_0$	2.04	1.59	1.44	0.78

the results calculated, the fluorescence intensity of S_1 in THF should be stronger than that in crystals. Nevertheless, the decay of the molecule in THF from CzS-CN-ax to CzS-CN-eq could induce weak fluorescence in

THF. Moreover, although the RMSD value becomes smaller, and this brings larger non-radiative decay rate for molecule in crystal compared with that in THF. Thus, this is the reason that the RMSD values are decreased significantly from THF solution to crystal state, while the calculated non-radiative decay rates in three crystals are much larger than that in the solution. Moreover, the mass center of the S_0 structure is coincided with that of the S_1 structure in our calculation. The phosphorescence rates for the molecule in crystals are much larger than that in THF, while the non-radiative rates of T_1 in both crystals and THF are in the same order of magnitude. It indicates that stronger phosphorescence emission in solid phase is due to enhanced phosphorescence rate, and AIE properties are confirmed. As the ISC process is also important for phosphorescence, the ISC rates between S_1 and T_N are calculated. It is found that the ISC rates between S_1 and T_1 are all smaller than that between S_1 and higher excited triplet states, which indicates that higher

Table 4

Calculated radiative and non-radiative rates (s^{-1}) from S_1 to S_0 and T_1 to S_0 as well as the ISC and RISC Rates (s^{-1}) between S_1 and T_N .

	Crystal A	Crystal B	Crystal C	THF
$K_r (S_1 \rightarrow S_0)$	5.83×10^7	5.70×10^7	4.21×10^7	4.18×10^8
$K_{nr} (S_1 \rightarrow S_0)$	4.89×10^9	2.32×10^9	3.94×10^9	7.67×10^7
$K_{ISC}(S_1 \rightarrow T_1)$	5.74×10^5	8.09×10^4	2.07×10^5	2.48×10^2
$K_{RISC}(T_1 \rightarrow S_1)$	5.82×10^{-13}	2.82×10^{-9}	9.17×10^{-12}	8.76×10^{-16}
$K_{ISC}(S_1 \rightarrow T_2)$	2.66×10^6	7.03×10^6	1.88×10^7	—
$K_{RISC}(T_2 \rightarrow S_1)$	4.66×10^{-5}	5.16×10^{-2}	0.43	—
$K_{ISC}(S_1 \rightarrow T_3)$	2.57×10^8	3.68×10^6	5.40×10^7	—
$K_{RISC}(T_3 \rightarrow S_1)$	5.48×10^{-3}	2.70×10^{-2}	1.33	—
$K_{ISC}(S_1 \rightarrow T_4)$	3.18×10^8	—	1.72×10^6	—
$K_{RISC}(T_4 \rightarrow S_1)$	3.49×10^5	—	2.47×10^4	—
$K_r(T_1 \rightarrow S_0)$	3.99×10^5	5.83×10^4	1.87×10^5	2.55×10^{-1}
$K_{nr}(T_1 \rightarrow S_0)$	2.15×10^6	4.08×10^6	1.34×10^6	2.77×10^6

excited states are favorable for phosphorescence. The RISC rates between T_4 and S_1 calculated in crystals may also go against the phosphorescence to a certain extent. Due to the unavailability of higher excited triplet states in THF, the ISC rates between S_1 and T_N in THF is not calculated here.

In order to investigate the non-radiative energy consumption process of excited state, two indexes: the Huang-Rhys (HR) factor and the reorganization energy are selected and calculated. The HR factor can be written as $HR_k = \frac{\omega_k^2 D_k^2}{2}$, where ω_k is the vibration frequency and D_k is the normal coordinate displacement of mode k . The HR factors versus the normal-mode frequencies for T_1 in THF and solid phase are illustrated in

Fig. 8. The HR factors in the solid phase (Fig. 8(b)) are smaller than that in THF (Fig. 8(a)), especially for these in the low-frequency regions ($<500 \text{ cm}^{-1}$). Large values of the HR factor for CzS-CN in THF are all in the lower frequency regions such as 9.5 (with vibration mode at 31.5 cm^{-1}), 0.55 (483.9 cm^{-1}), and 0.34 (935.0 cm^{-1}). HR factors for CzS-CN in the solid phase are all reduced with the largest three values being 1.4 (with vibration mode at 88.2 cm^{-1}), 0.7 (239.1 cm^{-1}), and 0.5 (1670.9 cm^{-1}). They correspond to the rotation of the dihedral angles as shown in the insets. Furthermore, the reorganization energy contributed by vibration modes in THF and in solid phase is shown in Fig. 8(c) and (d) respectively. It is found that the reorganization energy contributed by low-frequency modes changes slightly. The moderate-frequency (at about 1500 cm^{-1}) vibration modes have a little more significant contribution to the reorganization energy in crystals than in solvent. In addition, the high-frequency modes show some contribution to the reorganization energy. The total reorganization energy of CzS-CN in THF is 454 meV , while it decreases to 424 meV , 370 meV and 301 meV in Crystal A, B and C respectively. The contributions from bond length, bond angle and dihedral angle to the total reorganization energy are shown in Fig. 9. Results show that the bond length contribution to reorganization energies takes the major part with the ratio 75.47% in THF and 72.52%, 84.61% and 90.69% for crystal A, B and C respectively. As for dihedral angle, the contribution is 23.19% in THF and it changes to 25.75%, 14.24% and 7.93% for crystal A, B and C respectively, the changes of contribution from dihedral angle are obvious, this shows that the restricted rotation motion plays an important role in determining photophysical properties. The energy in THF is larger than that in the solid phase, which means the non-radiative rate for the molecule in crystals may be smaller than that in THF. Nevertheless, the non-radiative rates for T_1 in crystals are in the same order of magnitude

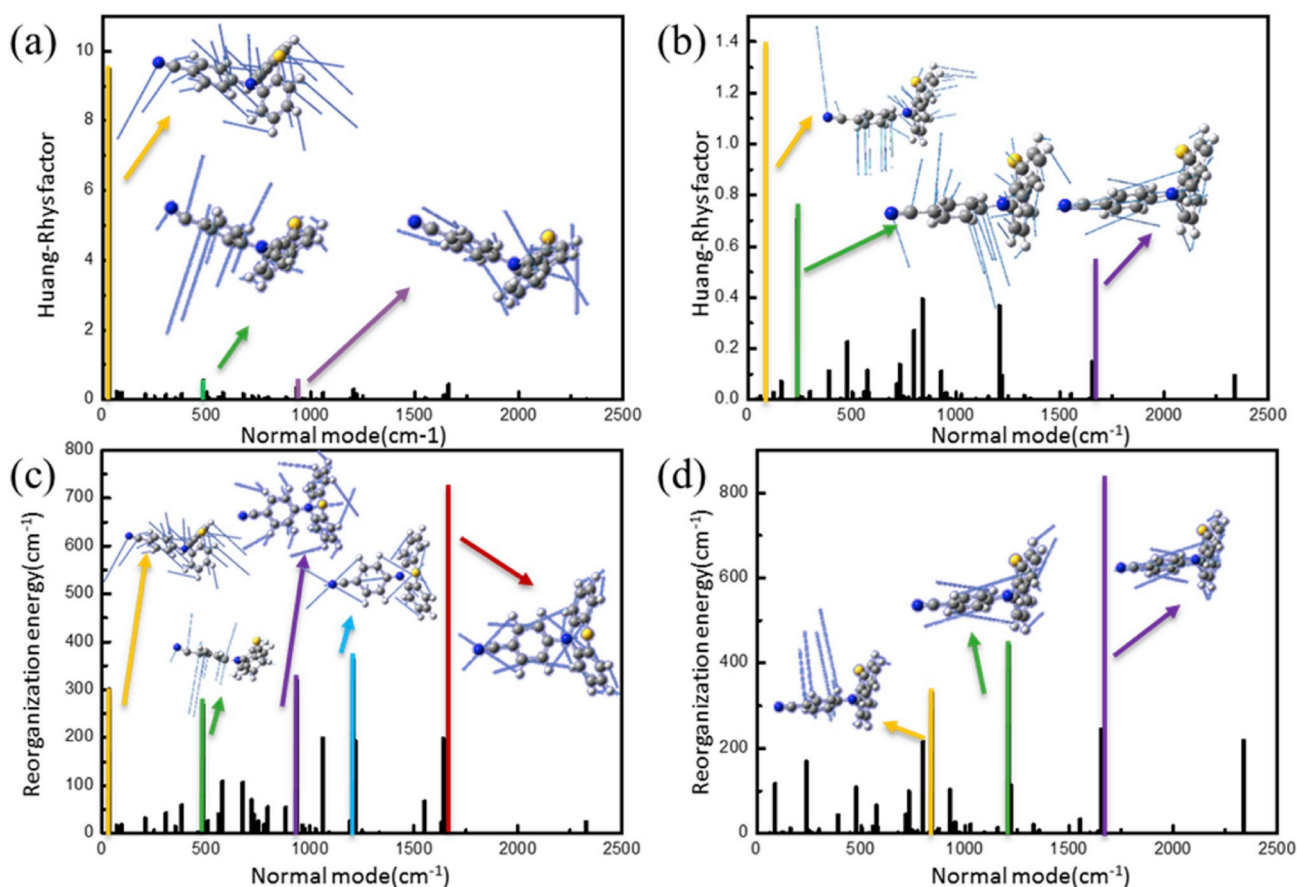


Fig. 8. Calculated HR factors versus the normal-mode frequencies in THF (a) and Crystal A (b) from T_1 to S_0 as well as the reorganization energies versus the normal-mode frequencies in THF (c) and Crystal A (d), respectively. Representative vibration modes are shown as insets.

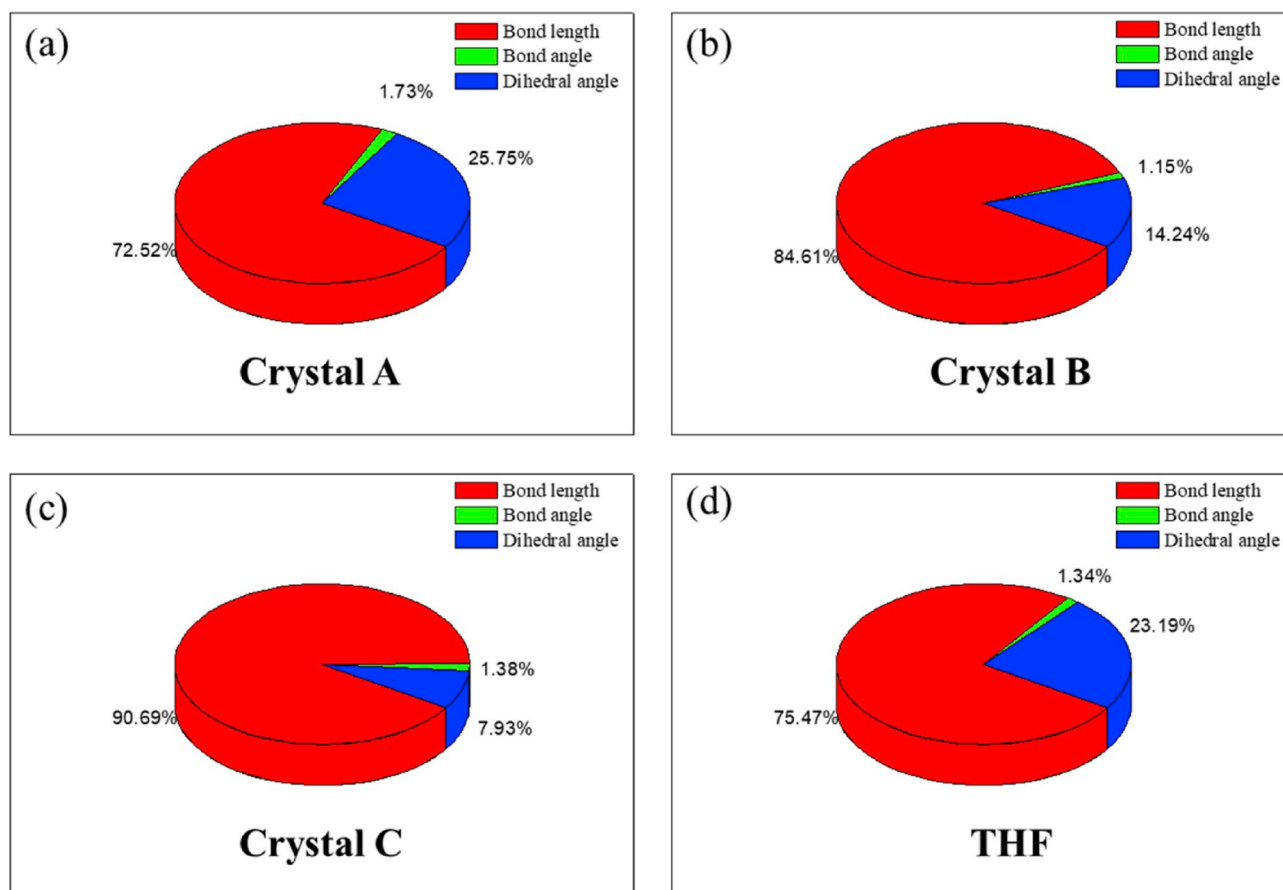


Fig. 9. Contribution ratios to the reorganization energy from bond length (red), bond angle (green) and dihedral angle (blue) of CzS-CN in crystal A, B, C and THF respectively. (For interpretation of the references to colour in this figure legend, the reader is referred to the Web version of this article.)

as that in THF (as shown in Table 4), which may be induced by different electron coupling in THF and in crystals.

4. Conclusion

In summary, the excited states properties of CzS-CN in three crystals and THF are theoretically studied by QM/MM and PCM methods respectively. Two stable structures (CzS-CN-ax and CzS-CN-eq) are found for the molecule in THF, while CzS-CN-ax is confirmed as the most stable geometry and it is responsible for the emission in THF. For the molecule in crystals, emissions in Crystal B and C are only contributed by single molecule, while dimers are confirmed to participate in emission for Crystal A based on the analysis of emission wavelengths and interaction energy. The excited-state decay rates for the molecule calculated in both crystals and in THF indicate that the AIE phenomenon of CzS-CN is mainly induced by the increased phosphorescence rates. In addition, different emission properties of the molecule in three crystals are found, although there are some discrepancies with experimental results. Our theoretical results provide reasonable explanation for experimental spectra and provide some deeper understanding for the inherent mechanism of aggregation induced RTP, which could promote the development of new RTP molecules with high efficiencies and long lifetimes.

Declaration of competing interest

There are no conflicts of interest to declare.

CRediT authorship contribution statement

Yuchen Zhang: Writing - original draft. **Yuying Ma:** Data curation. **Kai Zhang:** Data curation. **Chuan-Kui Wang:** Project administration. **Lili Lin:** Formal analysis. **Jianzhong Fan:** Writing - review & editing.

Acknowledgments

This work is supported by the National Natural Science Foundation of China (Grant Nos. 11874242, 11904210) and Shandong Provincial Natural Science Foundation, China (ZR2019MA056). Thanks to the supporting of Taishan Scholar Project of Shandong Province. Thanks to the supporting of the Project funded by China Postdoctoral Science Foundation (Grant No. 2018M642689). Great thanks to Professor Yi Luo, Zhigang Shuai and Qian Peng for their helpful suggestions in our calculation. Thanks to Professor Yingli Niu for his great help in the usage of MOMAP.

References

- [1] C.W. Tang, S.A. VanSlyke, *Appl. Phys. Lett.* 51 (1987) 913.
- [2] J.H. Jou, S. Kumar, A. Agrawal, T.H. Li, S. Sahoo, *J. Mater. Chem. C* 3 (2015) 2974.
- [3] K. Yoshida, T. Matsushima, H. Nakanotani, C. Adachi, *Org. Electron.* 31 (2016) 191.
- [4] Q. Zhang, B. Li, S. Huang, H. Nomura, H. Tanaka, C. Adachi, *Nat. Photonics* 8 (2014) 326.
- [5] H. Uoyama, K. Goushi, K. Shizu, H. Nomura, C. Adachi, *Nature* 492 (2012) 234.
- [6] L. Lin, Z. Wang, J. Fan, C.K. Wang, *Org. Electron.* 41 (2017) 17.
- [7] S. Hirata, K. Totani, J. Zhang, T. Yamashita, H. Kaji, S. Marder, T. Watanabe, C. Adachi, *Adv. Funct. Mater.* 23 (2013) 3386.
- [8] Z. Yang, Z. Mao, X. Zhang, D. Ou, Y. Mu, Y. Zhang, C. Zhao, S. Liu, Z. Chi, J. Xu, *Angew. Chem.* 55 (2016) 2181.

- [9] E. Lucenti, A. Forni, C. Botta, L. Carlucci, C. Giannini, D. Marinotto, A. Previtali, S. Righetto, E. Cariati, *J. Phys. Chem. Lett.* 8 (2017) 1894.
- [10] J. Qin, X. Li, F. Feng, Q. Pan, Y. Bai, J. Zhao, *Spectrochim. Acta A* 179 (2017) 233.
- [11] M. Kwon, D. Lee, S. Seo, J. Jung, J. Kim, *Angew. Chem.* 126 (2015) 11359.
- [12] J. Yang, X. Gao, Z. Xie, Y. Gong, M. Fang, Q. Peng, Z. Chi, Z. Li, *Angew. Chem. Int. Ed.* 129 (2017) 15299.
- [13] J. Wang, X. Gu, H. Ma, Q. Peng, X. Huang, X. Zheng, S. Sung, G. Shan, J. Lam, Z. Shuai, B. Tang, *Nat. Commun.* 9 (2018) 2963.
- [14] X. Ma, C. Xu, J. Wang, H. Tian, *Angew. Chem.* 130 (2018) 11020.
- [15] S. Cai, H. Shi, J. Li, L. Gu, Y. Ni, Z. Cheng, S. Wang, W. Xiong, L. Li, Z. An, W. Huang, *Adv. Mater.* 29 (2017) 1701244.
- [16] H. Ma, Q. Peng, Z. An, W. Huang, Z. Shuai, *J. Am. Chem. Soc.* 141 (2019) 1010.
- [17] H. Ma, A. Lv, L. Fu, S. Wang, Z. An, H. Shi, W. Huang, *Ann. Phys.-Berlin* 531 (2019) 1800482.
- [18] A. Lv, W. Ye, X. Jiang, N. Gan, H. Shi, W. Yao, H. Ma, Z. An, W. Huang, *J. Phys. Chem. Lett.* 10 (2019) 1037.
- [19] Z. He, H. Gao, S. Zhang, S. Zheng, Y. Wang, Z. Zhao, D. Ding, B. Yang, Y. Zhang, W. Z. Yuan, *Adv. Mater.* 31 (2019) 1807222.
- [20] H. Mieno, R. Kabe, N. Notsuka, M.D. Allendorf, C. Adachi, *Adv. Opt. Mater.* 4 (2016) 1015–1021.
- [21] X. Yang, D. Yan, *Adv. Opt. Mater.* 4 (2016) 897–905.
- [22] L. Bian, H. Shi, X. Wang, K. Ling, H. Ma, M. Li, Z. Cheng, C. Ma, S. Cai, Q. Wu, *J. Am. Chem. Soc.* 140 (2018) 10734–10739.
- [23] Q. Li, Y. Tang, W. Hu, Z. Li, *Small* 14 (2018) 1801560.
- [24] N. Gan, H. Shi, Z. An, W. Huang, *Adv. Funct. Mater.* 28 (2018) 1802657.
- [25] Y. Hong, J. Lam, B. Tang, *Chem. Soc. Rev.* 40 (2011) 5361.
- [26] J. Mei, N. Leung, C. Leung, R. Kwok, J. Lam, B. Tang, *Chem. Rev.* 115 (2015) 11718.
- [27] W.Z. Yuan, X.Y. Shen, H. Zhao, J.W. Lam, L. Tang, P. Lu, C. Wang, Y. Liu, Z. Wang, Q. Zheng, *J. Phys. Chem. C* 114 (2010) 6090–6099.
- [28] J. Yang, Z. Ren, Z. Xie, Y. Liu, C.K. Wang, Y. Xie, Q. Peng, B. Xu, W. Tian, F. Zhang, *Angew. Chem.* 129 (2016) 880.
- [29] Y. Xie, Y. Ge, P. Qian, C. Li, Q. Li, L. Zhen, *Adv. Mater.* 29 (2017) 1606829.
- [30] Q. Li, Z. Li, *Adv. Sci.* 4 (2017) 1600484.
- [31] J. Yang, L. Li, Y. Yu, Z. Ren, , Q.P., S. Ye, Q. Li, Z. Li, *Mater. Chem. Front.* 1 (2017) 91.
- [32] J. Yang, Z. Ren, B. Chen, M. Fang, Z. Zhao, B. Tang, Q. Peng, Z. Li, *J. Mater. Chem. C* 5 (2017) 9242.
- [33] B. Mennucci, *WIREs Comput. Mol. Sci.* 2 (2012) 386.
- [34] L. Cai, J. Fan, X. Kong, L. Lin, C.K. Wang, *Chin. Phys. B* 26 (2017) 118503.
- [35] L. Lin, J. Fan, C.K. Wang, *Org. Electron.* 51 (2017) 349.
- [36] J. Fan, Y. Zhang, K. Zhang, J. Liu, G. Jiang, F. Li, L. Lin, C.K. Wang, *J. Mater. Chem. C* 7 (2019) 8874.
- [37] J. Fan, Y. Zhang, K. Zhang, L. Lin, C.K. Wang, *J. Lumin.* 209 (2019) 372.
- [38] J. Liu, Y. Zhang, K. Zhang, J. Fan, C.K. Wang, L. Lin, *Org. Electron.* 71 (2019) 212.
- [39] L. Chung, W. Sameera, R. Ramozzi, A. Page, M. Hatanaka, G. Petrova, T. Harris, X. Li, Z. Ke, F. Liu, *Chem. Rev.* 115 (2015) 5678.
- [40] [a] M.J. Frisch, G.W. Trucks, H.B. Schlegel, G.E. Scuseria, M.A. Robb, J. R. Cheeseman, G. Scalmani, V. Barone, G.A. Petersson, H. Nakatsuji, X. Li, M. Caricato, A.V. Marenich, J. Bloino, B.G. Janesko, R. Gomperts, B. Mennucci, H. P. Hratchian, J.V. Ortiz, A.F. Izmaylov, J.L. Sonnenberg, Williams, F. Ding, F. Lipparini, F. Egidi, J. Goings, B. Peng, A. Petrone, T. Henderson, D. Ranasinghe, V.G. Zakrzewski, J. Gao, N. Rega, G. Zheng, W. Liang, M. Hada, M. Ehara, K. Toyota, R. Fukuda, J. Hasegawa, M. Ishida, T. Nakajima, Y. Honda, O. Kitao, H. Nakai, T. Vreven, K. Throssell, J.A. Montgomery Jr., J.E. Peralta, F. Ogliaro, M. J. Bearpark, J.J. Heyd, E.N. Brothers, K.N. Kudin, V.N. Staroverov, T.A. Keith, R. Kobayashi, J. Normand, K. Raghavachari, A.P. Rendell, J.C. Burant, S.S. Iyengar, J. Tomasi, M. Cossi, J.M. Millam, M. Klene, C. Adamo, R. Cammi, J.W. Ochterski, R.L. Martin, K. Morokuma, O. Farkas, J.B. Foresman, D.J. Fox, C.T. Wallingford, *Gaussian 16 Rev. A.03*, 2016; [b] Z. Shuai, Q. Peng, *Phys. Rep.* 537 (2014) 123.
- [41] [a] M. Rätsep, Z. Cai, J. Reimers, A. Freiberg, *J. Chem. Phys.* 134 (2011), 01B608; [b] Q. Peng, Y. Yi, Z. Shuai, J. Shao, *J. Chem. Phys.* 126 (2007) 1740.
- [42] Dalton, A molecular electronic structure program. <http://daltonprogram.org>.
- [43] Y. Niu, W. Li, Q. Peng, H. Geng, Y. Yi, L. Wang, G. Nan, D. Wang, Z. Shuai, *Mol. Phys.* 116 (2018) 1078.
- [44] Y. Niu, Q. Peng, Z. Shuai, *Sci. China Chem.* 51 (2008) 1153.
- [45] Q. Peng, Y. Yi, Z. Shuai, *J. Am. Chem. Soc.* 129 (2007) 9333.
- [46] P.K. Samanta, D. Kim, V. Coropceanu, J.L. Bredas, *J. Am. Chem. Soc.* 139 (2017) 4042.
- [47] X.K. Chen, D. Kim, J.L. Bredas, *Acc. Chem. Res.* 51 (2018) 2215.
- [48] R. Liu, X. Gao, M. Barbatti, J. Jiang, G. Zhang, *J. Phys. Chem. Lett.* 10 (2019) 1388.
- [49] T. Lu, F. Chen, *J. Comput. Chem.* 33 (2012) 580.
- [50] C. Lefebvre, G. Rubez, H. Khartabil, J. Boisson, J. Contreras-García, E. Hénon, *Phys. Chem. Chem. Phys.* 19 (2017) 17928.
- [51] O. Vahtras, H. Ågren, P. Jo/rgensen, H.J.R.A. Jensen, T. Helgaker, J. Olsen, *J. Chem. Phys.* 97 (1992) 9178.